Model for the Glauber-type calculations of beam fragmentation at low energies*

A. N. Ismailova[1,2,3†] Yu. L. Parfenova[1] P. G. Sharov[1,4] D. M. Janseitov[1,2]

[1]Flerov Laboratory of Nuclear Reactions, JINR, 20 Joliot Curie Str, Dubna, Russia
[2]Institute of Nuclear Physics, 1 Ibragimov Str, Almaty, Kazakhstan
[3]Al-Farabi Kazakh National University, Almaty, Kazakhstan
[4]Institute of Physics, Silesian University Opava, Czech Republic

Abstract: The Glauber-type model for description nuclear fragmentation in light targets at the energies below 100 A·MeV is suggested. It is developed on the basis of the Glauber model within the nucleon transparent limit where the Lorentz invariant phase space factor is introduced to account for the energy and momentum conservation laws. The region of applicability of the model is discussed. The longitudinal momentum distributions of the most neutron rich nuclei, ^{10}Be, ^{9}Li, ^{8}He, produced in few nucleon removal reactions in the ^{11}B fragmentation in the Be target at the beam energies 10, 30, and 100 A·MeV are calculated. The results of the calculations are compared with predictions of statistical models of fragmentation such as the Goldhaber model. Within the new model, the asymmetric longitudinal momentum distributions at low energies are explained by the kinematical locus and geometry of the reaction.

Keywords: Glauber model, fragmentation, breakup reactions, momentum distributions

DOI: **CSTR:**

I. INTRODUCTION

In-flight method is widely used in experimental nuclear studies for radioactive ion beam production. The primary beam is used to generate a specific nucleus in a target, and this nucleus should be separated from other products in a fragment separator. For effective operation of the fragment separator knowledge of the longitudinal momentum distributions of the nucleus is of importance.

There are many nuclear research centers working with low-energy ($E < 100$ A·MeV) radioactive beams using the in-flight method, such as FLNR (JINR, Russia) [1], FRIB (Michigan State University (MSU), USA) [2], GANIL (France) [3], RNC (RIKEN, Japan) [4], and INFN-LNS (Italy) [5]. These are the energy ranges where studies of the exotic nuclear structure in direct reactions are available.

Experimental data show a significant qualitative difference in the momentum distributions of fragments at low energies compared to those obtained at higher energies. The distributions exhibit asymmetry and the position of the maximum of the distributions changes with different fragments. In this context, understanding of mechanisms of fragmentation becomes particularly important.

Note that the in-flight method is based on the assumption that the longitudinal momentum P_{beam} distributions of the fragments are narrow and focused around the longitudinal momentum corresponding to the beam velocity. This paper demonstrates that, at low energies the longitudinal momenta of the fragments may significantly deviate from P_{beam}. Thus, an approach is needed to relate the width and position of the longitudinal momentum distribution peak to the transferred momentum. The next example illustrates this problem. At the energy 30 A·MeV typical for the beams in FLNR, the longitudinal emittence of the initial beam 2% leads to that of about 20% after the fragmentation [1], and the fragments are accepted into the secondary beam within a narrow region of the longitudinal momentum distribution. The optimal acceptance is achieved when the fragments momenta are close to the peak of the longitudinal momentum distribution [6].

The Glauber model is the most widely used universal approach for this kind of calculations which provides a satisfactory description of experimental data at intermediate and high energies, $E > 100$ A·MeV. At energies below 100 A·MeV the applicability of the Glauber model becomes ambiguous. For now, the experimental data on the nuclear fragmentation at the energies $E < 100$ A·MeV are accumulated, different parametrizations are suggested for description of the fragment energies and angular

Received 3 December 2024; Accepted 26 January 2025

* This work has been supported by the Science Committee of the Ministry of Science and Higher Education of the Republic of Kazakhstan (AP19678586)

† E-mail: ismailova@jinr.ru

distributions, that call for a simple model of the Glauber type extended for the calculations at the energies, where the transferred momentum and the beam momentum are of the same order of the magnitude. We propose an approach based on the Glauber model that accounts for energy and momentum conservation laws while maintaining its simplicity and transparency.

In this approach, it is possible to get an analytical expression for the amplitude of the process, and correct it using the Lorentz invariant phase volume, thus accounting for the conservation laws.

In the present paper we introduce this model, analyze the region of its applicability, and apply the suggested approach for the calculations of the ^{11}B fragmentation in the Be target.

Note that ^{11}B is the lightest nucleus for which a few-proton removal process leads to the production of ^{10}Be,^{9}Li, and ^{8}He fragments. All these nuclear fragments have been thoroughly studied experimentally, providing input parameters for our approach. We analyze the changes in the phase volume and the longitudinal momentum distributions as functions of the beam energy and the mass number of the fragments. We compare the momentum distributions with those obtained using systematics widely used fragmentation calculations (see Refs. [7, 8]).

All the calculations of the momentum distributions and cross sections were performed using the Monte-Carlo method.

II. MODEL DESCRIPTION

In general case, the differential cross section of the process with n bodies in the final state is expressed as

$$d\sigma = \frac{|T|^2}{v} dV^{(n)} \tag{1}$$

where T denotes the T-matrix, v is the beam velocity, and $dV^{(n)}$ is the phase volume of the n-body system of fragments.

We propose an approach where, instead of the T-matrix, we use the inelastic scattering amplitude obtained in the Glauber method, while preserving the Lorentz-invariant phase volume. Using this procedure, we formally provide the conservation of energy and momenta; however, we expect a qualitative description of the correlations and momentum distributions. Nevertheless, such an approach may describe the influence of the Q-value and other purely kinematical effects (which may be significant at low energies) on the momentum distribution of the fragments.

We consider the process of fragmentation of the projectile (P) in the target (T) (Figure 1) assuming that the projectile consists of the n fragments, which are relatively heavy core (C) and nucleons. We consider this problem in the projectile rest frame.

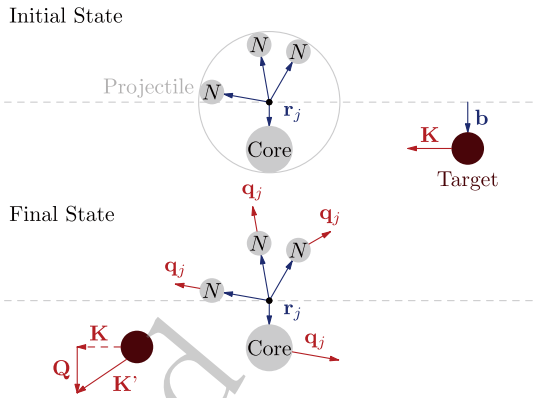

Fig. 1. (color online) Kinematical scheme of the fragmentation reaction and kinematical variables in the projectile rest frame used in the model.

A. Inelastic scattering amplitude and factorization

The inelastic scattering amplitude of this process can be written as the integral over impact parameter $\mathbf{b}$ and the coordinates of the preformed clusters $\mathbf{r}_j$:

$$\mathcal{F}_{fi} = \frac{k}{2\pi i} \int e^{i\mathbf{Q}\cdot\mathbf{b}} d^2\mathbf{b} \int \prod_{k=1}^{n} d^3\mathbf{r}_k \times \Psi_F^* \left[\prod_{j=1}^{n} S_j(\mathbf{b}-\mathbf{t}_j) - 1 \right] \Psi_I, \tag{2}$$

where S_j is the profile function of the fragment-target (core-target $j=C$ and nucleon-target $j=N$) interaction obtained using the optical model potential (see Eq. (9)); $\mathbf{t}_j$ is the projection of the $\mathbf{r}_j$ on the impact parameter plain (orthogonal to $\mathbf{K}$)

$$\mathbf{t}_j = \mathbf{r}_j - (\mathbf{r}_j \cdot \mathbf{K})\mathbf{K}/K^2;$$

Ψ_I is the projectile initial state wave function (WF) of the relative motion of the fragments with coordinates $\mathbf{r}_j$ (indices j denote the core and nucleon fragments)

$$\Psi_I \equiv \Psi_I(\mathbf{r}_1, \ldots, \mathbf{r}_n);$$

Ψ_F is the final state WF defined by the fragments' coordinates and momenta.

$$\Psi_F \equiv \Psi_F(\mathbf{r}_1, \ldots, \mathbf{r}_n, \mathbf{q}_1, \ldots, \mathbf{q}_n).$$

As we consider the problem in the projectile rest frame, $\mathbf{K}$ and $\mathbf{K}'$ are the initial and final target momenta,

respectively. $\mathbf{Q}$ represents the target transferred momentum, while $\mathbf{q}_j$ are the fragment momenta after scattering in the projectile rest frame. Additionally, $\mathbf{q}_j$ can be interpreted as transferred momenta of the fragments.

With the single scattering approximation in Eq. (2) we get sum:

$$\mathcal{F}_{fi} = \sum_{j=1}^{n} f_j(\mathbf{Q}) \int (\Psi_F)^* e^{i\mathbf{Q}\mathbf{r}_j} \Psi_I \prod_{k=1}^{n} d^3\mathbf{r}_k, \tag{3}$$

where $f_j(\mathbf{Q})$ is the fragment-target elastic scattering amplitude [9]. And in the transparent nucleon limit $S_N = 1$ Eq. (3) reduces to the form:

$$\mathcal{F}_{fi} = f_C(\mathbf{Q}) \int (\Psi_F)^* e^{i\mathbf{Q}\mathbf{r}_C} \Psi_I \prod_{k=1}^{n} d^3\mathbf{r}_k, \tag{4}$$

Our next assumption concerns the factorization of the WF of the initial and final states

$$\Psi_I \to \prod_{j=1}^{N} \Psi_{Ij}(\mathbf{r}_j)$$

and

$$\Psi_F \to \prod_{j=1}^{N} \Psi_{Fj}(\mathbf{r}_j, \mathbf{q}_j) \to \prod_{j=1}^{N} \exp[i\mathbf{r}_j\mathbf{q}_j].$$

Introducing the functions

$$F_j(\mathbf{Q}, \mathbf{q}_1, \ldots, \mathbf{q}_n) = \int d^3\mathbf{r}_j e^{i\mathbf{Q}\mathbf{r}_j} \Psi^*_{Fj}(\mathbf{r}_j, \mathbf{q}_j) \Psi_{Ij}(\mathbf{r}_j) \times \prod_{k\neq j} \int d^3\mathbf{r}_k \Psi^*_{Fk}(\mathbf{r}_k, \mathbf{q}_k) \Psi_{Ik}(\mathbf{r}_k). \tag{5}$$

and assuming that the final state WFs can be approximated by plane waves, we obtain

$$\begin{aligned} F_j(\mathbf{Q}, \mathbf{q}_1, \ldots, \mathbf{q}_N) &= \int d^3\mathbf{r}_j e^{-i(\mathbf{q}_j - \mathbf{Q})\mathbf{r}_j} \Psi_{Ij}(\mathbf{r}_j) \\ &\times \prod_{k\neq j} \int d^3\mathbf{r}_k e^{-i\mathbf{q}_k\mathbf{r}_j} \Psi_{Ik}(\mathbf{r}_k) \\ &= F_j(\mathbf{q}_j - \mathbf{Q}) \prod_{k\neq j} F_k(\mathbf{q}_k). \end{aligned} \tag{6}$$

Substitution of Eq. (6) into Eq. (4) gives the amplitude of inelastic scattering, written as

$$\mathcal{F}_{fi} = f_C(\mathbf{Q}) F_C(\mathbf{q}_C - \mathbf{Q}) \prod_{k} F_N(\mathbf{q}_k), \tag{7}$$

Note that $\mathbf{Q}$ and $\mathbf{q}_j$ in Eq. (2) are assumed to lie in the plane orthogonal to the momentum $\mathbf{K}$. However, if we assume F_j and the core-fragment potential to be central-symmetric one, the dependence of $\mathcal{F}_{if}$ on the directions of $\mathbf{Q}$ and $\mathbf{q}_j$ should be minimal, making the use of Eq. (7) reasonable.

F_C and F_N in Eq. (7) represent the form factors determined by the nucleus size. Thus, the amplitude of inelastic scattering is defined by the elastic scattering amplitude of the core $f_C(\mathbf{Q})$.

With the oscillator WF

$$\left(\frac{54}{\pi}\right)^{1/4} r_j^{-3/2} r \exp\left(-\frac{3r^2}{4r_j^2}\right)$$

we obtain expression for the form factors F_j

$$F_j(q) = \sqrt[4]{\frac{32}{27}\pi\langle r_j\rangle^6 e^{-\frac{4}{3}q^2\langle r_j\rangle^2}}; \tag{8}$$

where $\langle r_j\rangle$ is the root mean square (RMS) distance of fragment j from the center of mass of the projectile.

Note that the parameters of the approach include the RMS radii of the fragments and the related RMS distance between each fragment and the center of mass of the projectile.

B. Profile functions

The elastic scattering amplitudes $f_C(\mathbf{Q})$ and $f_N(\mathbf{Q})$ are calculated in the Glauber model using the corresponding core-target profile function S_j.

In our calculations, the profile functions of the core-target interaction are derived using the model potential:

$$S_j(b) = \exp\left[-\frac{i}{\hbar v}\int_{-\infty}^{\infty} dz\, V_j\left(\sqrt{b^2+z^2}\right)\right], \tag{9}$$

where $r = \sqrt{b^2+z^2}$ and $V_j(r)$ is the optical model potential for the core-target or nucleon-target interaction, b is the impact parameter of the center of mass of the fragment (see, for example, Refs. [10, 11]), v is the beam velocity, and z is the coordinate along the beam axis.

To perform the calculations over a wide energy range (from 10 to 100 A·MeV), we use the standard parametrization of the nucleon-nucleon interaction potential with the parameters from Refs. [12, 13], which are valid for the incident energy range from 10 to 2000 A·MeV. The optical potential of the core-target interaction is found as the folding [14] of the potential with the core density distribution.

The core-target interaction potential is expressed by:

$$V_C(\mathbf{r}) = \int A_C \rho_C(\mathbf{r}') \overline{V_C}(|\mathbf{r}-\mathbf{r}'|)\, d\mathbf{r}', \tag{10}$$

where A_C is the core mass number, ρ_C is the core density distribution and $\overline{V_C}(|\mathbf{r}-\mathbf{r}'|)$ represents the effective interaction potential, and:

$$\overline{V_{CT}}(|\mathbf{r}-\mathbf{r}'|) = -\frac{i}{2}\hbar v A_T \rho_T(|\mathbf{r}-\mathbf{r}'|)\overline{\sigma_{NN}} \tag{11}$$

The density distributions of the interacting nuclear systems are approximated by the Gaussian distribution [15] as

$$\rho(x) = \rho_0 \exp(-\alpha x^2), \tag{12}$$

where $\alpha = \left[\frac{2}{3}\langle r^2\rangle\right]^{-1}$ is the density distribution parameter related to RMS radius of the nucleus $\langle r^2\rangle^{1/2}$, and $\rho(x)$ is normalized to unity. $\overline{\sigma}_{NN}$ is the nucleon-nucleon cross-section averaged over the number of neutrons and protons involved in the interaction (for more details see Ref. [12, 13]).

III. RESULTS AND DISCUSSION

Studying fragmentation of ^{11}B, we consider three reactions leading to production of the ^{10}Be, ^{9}Li, ^{8}He isotopes

$$^{11}\mathrm{B} + {}^{9}\mathrm{Be} \rightarrow {}^{9}\mathrm{Be} + {}^{10}\mathrm{Be} + p,$$
$$^{11}\mathrm{B} + {}^{9}\mathrm{Be} \rightarrow {}^{9}\mathrm{Be} + {}^{9}\mathrm{Li} + 2p,$$
$$^{11}\mathrm{B} + {}^{9}\mathrm{Be} \rightarrow {}^{9}\mathrm{Be} + {}^{8}\mathrm{He} + 3p,$$

which illustrate the "path" towards the neutron dripline. Calculations are performed for the beam energies 10, 30, and 100 A·MeV, demonstrating the changes in the differential elastic cross section and the longitudinal momentum distributions of the core fragment as functions of the incident energy. The Monte-Carlo method is used to calculate the corresponding momentum distributions.

A. Elastic cross sections

Figure 2 illustrates the differential elastic cross section as a function of the transferred momenta q_j for protons ($j = p$) and the core fragments ($j = C$, where C corresponds to ^{10}Be, ^{9}Li, and ^{8}He, respectively) on a Be target for the incident energies 10, 30, and 100 A·MeV. The calculated proton cross sections are smaller than the core cross sections by a few orders of magnitude and the corresponding amplitudes satisfy $f_C \gg f_N$, indicating that the core-target interaction dominates over the nucleon-target interaction. One can also see from Figure 2 that the nucleon transfer can occur with the momentum transfer significantly exceeding the value corresponding to the first diffraction minimum. In the calculations of the elastic scattering, we assume that the dominant contribution to the elastic scattering cross section corresponds to the transferred momenta smaller than those at the first diffraction minimum (see Figure 2).

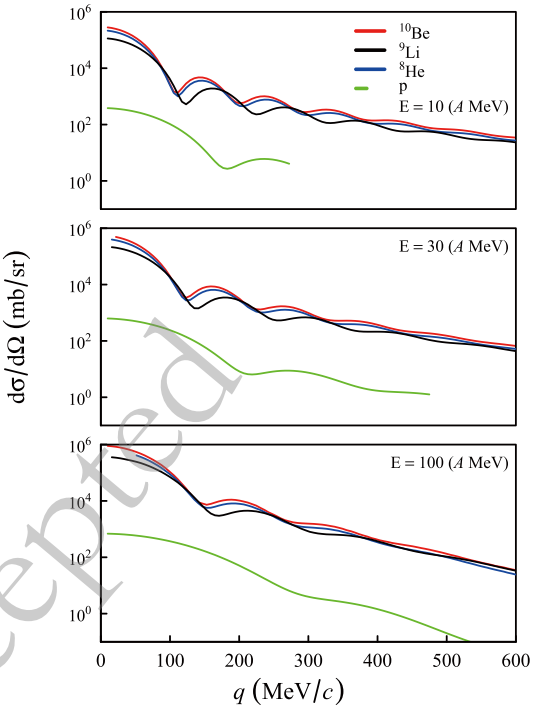

Fig. 2. (color online) Differential elastic scattering cross sections as functions of the transferred momentum q for protons and heavy ions (^{10}Be, ^{9}Li, and ^{8}He) scattered on a ^{9}Be target at different projectile energies (see legends in the panels).

As noted above, in our model, the projectile nucleus ^{11}B is treated as a system of a pre-formed heavy cluster and valence protons. The structure of ^{11}B is characterized by the form factor $F_C(\mathbf{q}_C)$ in Eq. (8), which is determined by the RMS distance of the core in ^{11}B. In our calculations, we use the RMS distance of proton $\langle r_p\rangle = 2.43$ fm determined by the standard charge radius systematics $1.2\times A^{1/3}$. As a first approximation, the RMS distance of the core $\langle r_C\rangle$ can be calculated assuming to be a point particle.

In the general case, the core WF in ^{11}B may be more complex, resulting in variations in $\langle r_C\rangle$. To demonstrate the sensitivity of our results to this parameter, we vary $\langle r_C\rangle$ (see Table 1) from the minimal value, corresponding to a more central impact, to the maximal value, representing a more peripheral interaction. The values of $\langle r_C\rangle$ are presented in the Table 1.

B. Momentum distributions

Figure 3 shows the correlation plots of the target transferred momentum (Q) versus the projection q_{Cz} of the core momentum q_C on the z-axis, coinciding with the

Table 1. The RMS distances of heavy fragments used in the calculations. $\langle r_c \rangle$ is the default value; $\min\langle r_c \rangle$ represents the radius for the 'more central' reaction; $\max\langle r_c \rangle$ represents the radius for the 'more peripheral' reaction. All values are given in fm

Fragment	$\langle r_c \rangle$	$\min\langle r_c \rangle$	$\max\langle r_c \rangle$
^{10}Be	0.24	0.12	0.49
^{9}Li	0.49	0.24	0.97
^{8}He	0.73	0.36	1.46

beam direction. The calculations are performed for beam energies 10, 30, and 100 A·MeV and for different core fragments ^{10}Be, ^{9}Li, and ^{8}He.

It can be observed that at low beam energies (10 and 30 A·MeV), the variables Q and q_{Cz} exhibit strong correlation. This correlation weakens with increase in of removed nucleons.

Note that the kinematic locus includes only non-zeroth transferred momentum Q, since part of the beam energy is spent on nucleon knock-out. Therefore, the Serber model, introduced in Ref. [16], which is valid in the limit $Q = 0$ MeV/c, is not applicable in this case, and the core fragments appear to move slower than the beam nuclei. The Serber model describes the fragmentation process as a sudden removal of nucleons from the nucleus. In this model, the longitudinal momentum distribution of the fragments is determined by the initial wave function of the system, represented through the form factor of the initial state. One can see that (7) for the case of $Q \ll q_C$ reduces to the Serber model.

At high energy (100 A·MeV), the effect of "slowing down" is less pronounced, and the correlation becomes more symmetric with respect to $q_{Cz} = 0$, approaching to the predictions of the Serber model. However, the case $Q \ll q_C$ is still not realized. We plan to discuss the kinematic conditions under which our approach is reduced to the Serber model in perspective works.

In Figure 4, we present the correlation between the two projections of the core momentum in the projectile rest frame (q_{Cx} and q_{Cz}).

The kinematical loci of the fragments are clearly visible in these plots, and the loci of q_{Cz} are asymmetric relative to the beam momentum ($q_{Cz} = 0$). This indicates a tendency for the fragments to "slow down" at low energies relative to the beam velocity, which is related to the reaction kinematics.

This result demonstrates significant changes in the shape of the longitudinal momentum distributions with varying the beam energy, highlighting the importance of considering momentum and energy conservation laws. From this view point, the models assuming the sudden removal with $Q \to 0$, such as the Serber model and the traditional eikonal approximation of the Glauber model, provide only a qualitative description of the momentum distributions. At high energies, these models offer a good quantitative description of the cross sections; however, at energies below 100 A·MeV, they do not provide a correct description of the momentum distributions.

At higher energies, where the transferred momentum is much smaller than the beam momentum and can be

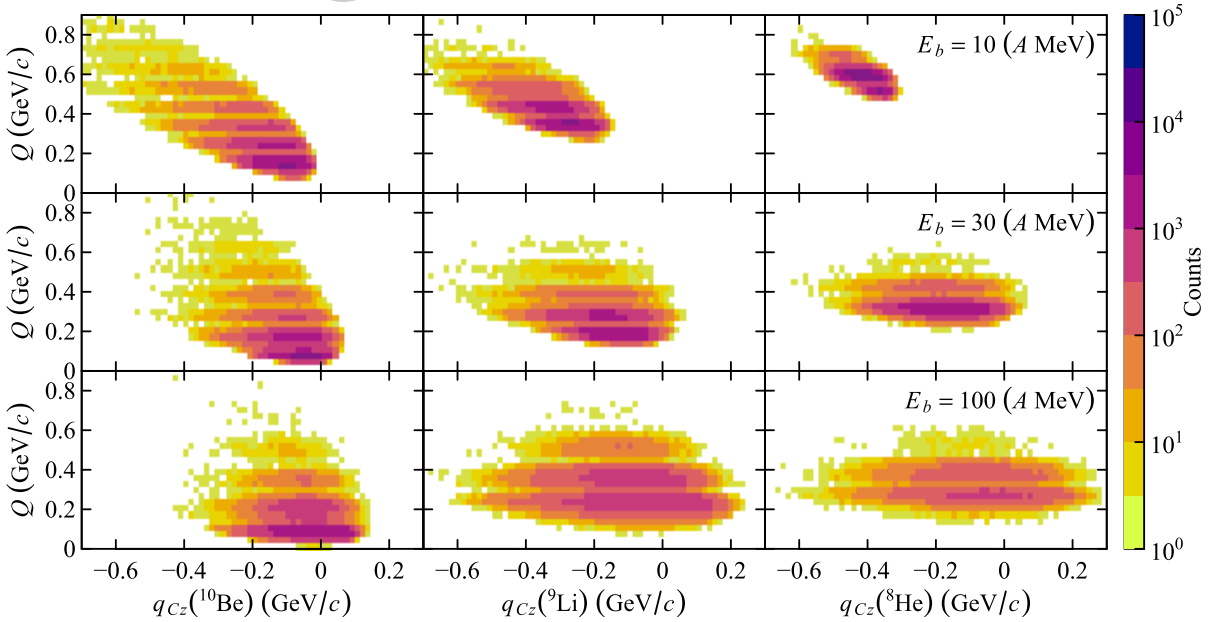

Fig. 3. (color online) Correlation between the transferred momentum of the target (Q) and the longitudinal component of the core momentum (q_{Cz}) in the projectile rest frame, obtained using the Monte Carlo method for different fragments (columns) and the ^{11}B beam energies (rows). The color palette indicates the number of events in the Monte Carlo calculations.

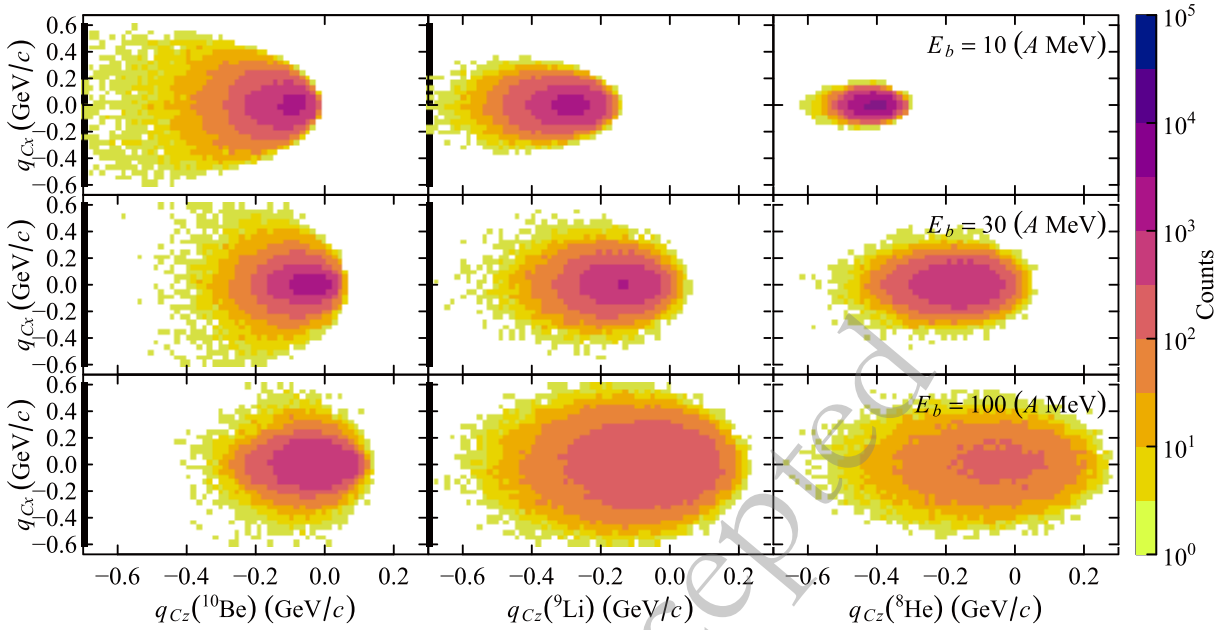

Fig. 4. (color online) Correlation between the transverse (q_{Cx}) and longitudinal (q_{Cz}) components of the core momentum in the projectile rest frame, obtained using the Monte Carlo method. The layout is the same as in Figure 3. The color palette indicates the number of events in the Monte Carlo calculations.

neglected, our model approaches the results obtained in the Glauber model in the transparent proton limit.

The sensitivity of our calculations to the $\langle r_C \rangle$ parameter is illustrated in Figure 5, where we present the characteristics of the longitudinal momentum distributions such as the peak position, standard deviation (SD), and skewness of the q_{Cz} distribution.

One can see that the peak position in the momentum distributions shifts to higher values with increase in the mass of the fragment. The skewness decreases as the fragment mass increases. The standard deviation of the longitudinal momentum distribution varies depending on the type of fragment.

The plots indicate that in peripheral reactions, the fragment can move faster than the projectile. Additionally, a narrowing of the q_{Cz} distribution is observed. In central interactions, the q_{Cz} distribution becomes wider and more asymmetric. Thus, more peripheral reactions produce faster fragments, while central reactions result in slower fragments relative to the beam velocity.

Finally, in Figure 6, we compare the calculated widths of the longitudinal momentum distributions of the fragments with predictions from the widely used Goldhaber model [7]. Following the approach outlined in this article, the standard deviation

$$\mathrm{SD} = \sqrt{\sigma^2} = \sqrt{m_N k T \frac{K(A-K)}{A}}$$

where A is the mass of the incident particle ^{11}B, and K is the mass of the fragment (^{10}Be, ^{9}Li, ^{8}He). The temperature T and Boltzmann constant k define σ^2 describing both the mean excitation energy transferred to the fragment during nuclear decay and the width of the fragment mo-

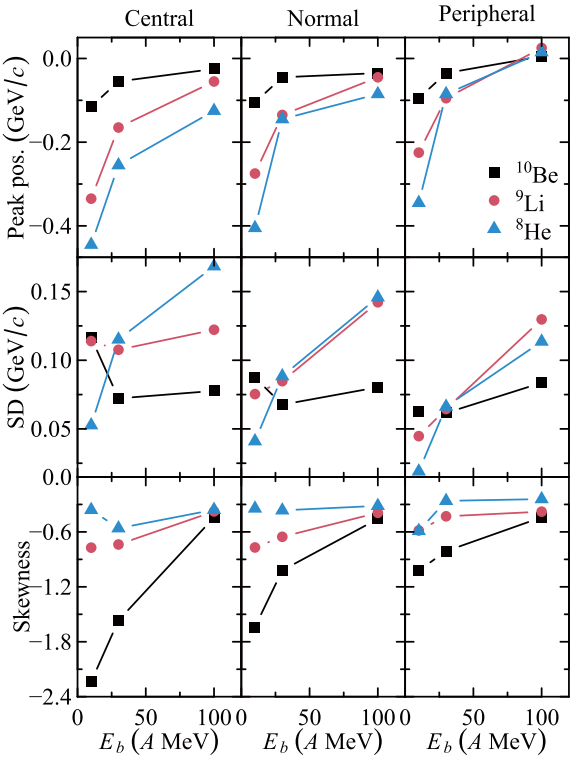

Fig. 5. (color online) The mode (peak position), standard deviation (SD), and skewness for different values of $\langle r_C \rangle$ (see Table 1).

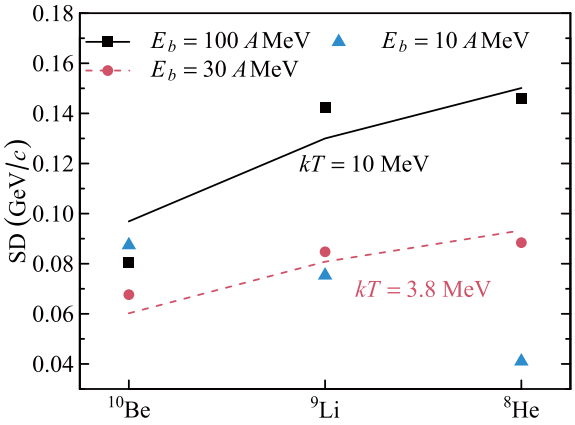

Fig. 6. (color online) Comparison of the standard deviation (SD) of q_{Cz} obtained in our calculations (points) with the predictions of the model from Ref. [7] (lines). The values of kT for the beam energies $E_b = 100$ A MeV and $E_b = 30$ A MeV are shown in the panels

mentum distribution.

For high beam energies ($E_b = 100$ A MeV and $E_b = 30$ A MeV), our results show reasonable agreement with the predictions of Ref. [7]. At low beam energy ($E_b = 10$ A MeV), the dependence of the longitudinal momentum distribution widths on the fragment mass number in our calculations qualitatively differs from that in Ref. [7], highlighting the limitations of the Goldhaber model and emphasizing the applicability of our proposed approach.

IV. SUMMARY

We suggest an approach based on the Glauber model, modified to account for energy and momentum conservation laws.

Using the example of ^{11}B fragmentation, we calculate the longitudinal momentum distributions of the ^{10}Be, ^{9}Li, and ^{8}He fragments. All results are obtained within the transparent proton limit. At the energies above $100A\cdot$MeV, our model produces results close to those obtained in the transparent proton limit ($S_N = 1$) of the eikonal approximation of the Glauber model. Additionally, the precision of the approach improves with increase in the heavy fragment mass.

At low energies, the peak position of the longitudinal momentum distribution increases as the core mass decreases. We also show that at energies below $100A\cdot$MeV, the fragments move slower than the beam nuclei, as defined by the kinematic locus, whereas at higher energies ($E > 100A\cdot$MeV), the fragments may move either faster or slower depending on the reaction geometry.

Account the energy and momentum conservation laws leads to significant changes in the shape of the longitudinal momentum distributions, causing asymmetry, where the low-momentum tail forms due to the large transferred momentum. Thus, compared to the Glauber model, our approach describes fragmentation over a wider range of momentum transfer.

Comparison with calculations from other models and parametrizations shows that at energies below $100A\cdot$MeV, kinematical loci and energy-momentum conservation laws must be taken into account when planning experiments and determining optimal conditions for fragment production.

References

[1] A. S. Fomichev, L. V. Grigorenko, S. A. Krupko, *et al.*, Eur. Phys. J. A **54**(6), 97 (2018)
[2] FRIB, https: //frib.msu.edu/, retrieved 15th December 2024.
[3] GANIL, http://ganil-spiral2.eu/, retrieved 15th December 2024.
[4] RIKEN, https: //www.riken.jp/en/research/labs/rnc/, retrieved 15th December 2024.
[5] G. Cuttone, L. Celona, F. Chines, *et al.*, Nucl. Instrum. Methods Phys. Res. B **261**(1), 1040 (2007)
[6] S. A. Krupko, S. G. Belogurov, A. A. Bezbakh, *et al.*, Phys. Part. Nucl. Lett. **21**(4), 902 (2024)
[7] A. S. Goldhaber, Phys. Lett. B **53**(4), 306 (1974)
[8] D. J. Morrissey, Phys. Rev. C **39**(2), 460 (1989)
[9] R. J. Glauber *High-energy collision theory*. pp. 83-182 (1987).
[10] K. Hencken, G. Bertsch, H. Esbensen, Phys. Rev. C **54**(6), 3043 (1996)
[11] Yu. L. Parfenova, M. V. Zhukov, J. S. Vaagen, Phys. Rev. C **62**(4), 044602 (2000)
[12] S. K. Charagi, S. K. Gupta, Phys. Rev. C **41**(4), 1610 (1990)
[13] L. Ray, Phys. Rev. C **20**(5), 1857 (1979)
[14] R. L. Varner, W. J. Thompson, T. L. McAbee, *et al.*, Phys. Rep. **201**, 57 (1991)
[15] Yu. L. Parfenova, M. V. Zhukov, Phys. Rev. C **66**(6), 064607 (2002)
[16] R. Serber, Phys. Rev. **72**(11), 1008 (1947)